ChemComm

Oxygen-atom Vacancy Formation and Reactivity in Polyoxovanadate Clusters

Journal:	*ChemComm*
Manuscript ID	CC-FEA-09-2020-005920
Article Type:	Feature Article

ARTICLE

Oxygen-atom Vacancy Formation and Reactivity in Polyoxovanadate Clusters

Received 00th January 20xx,
Accepted 00th January 20xx

DOI: 10.1039/x0xx00000x

Brittney E. Petel*[a] and Ellen M. Matson*[a]

Reducible metal oxides (RMOs) are widely used materials in heterogeneous catalysis due to their ability to facilitate the conversion of energy-poor substrates to energy-rich chemical fuels and feedstocks. Theoretical investigations have modeled the role of RMOs in catalysis and found they traditionally follow a mechanism in which the generation of oxygen-atom vacancies is crucial for the high activity of these solid supports. However, limited spectroscopic techniques for *in situ* analysis renders the identification of the reactivity of individual oxygen-atom vacancies on RMOs challenging. These obstacles can be circumvented through the use of homogenous complexes as molecular models for metal oxides, such as polyoxometalates. Summarized herein, a sub-class of polyoxometalates, polyoxovanadate-alkoxide clusters, ($[V_6O_7(OR)_{12}]^n$; R = CH_3, C_2H_5; n = 1-, 0, 1+), are explored as homogenous molecular models for bulk vanadium oxide. A series of synthetic strategies have been employed to access oxygen-deficient vanadium oxide assemblies, including addition of $V(Mes)_3(thf)$, tertiary phosphanes, and organic acids to plenary Lindqvist motifs. We further detail investigations surrounding the ability of these oxygen-deficient sites to mediate reductive transformations such as O_2 and NO_x^{1-} (x = 2, 3) activation.

Introduction

Reducible metal oxides (RMOs) are materials composed of redox active metal centers (e.g. Ti, V, Fe, Ce) capable of fluctuating between multiple oxidation states.[1-3] These materials are widely used as functional components in industrially relevant processes, including energy-based applications,[4-6] biomass conversion to commodity chemicals,[7-9] and in the remediation of environmental contaminants.[10-14] Furthermore, owing to the modular nature of these metal oxides (i.e. tunable atomic composition which influences the chemical, physical, and electronic properties of these materials), these solid supports are well-established to catalyze various chemical transformations with high turnover numbers and/or selectivity.[2, 15, 16]

Given the widespread applicability of these extended solids, researchers have become interested in analyzing the reactive components of RMOs. Through this work, oxygen-atom vacancies, located at the surface of the material, have been identified as the active sites in catalysis.[2, 17-19] These defects play a central role in the most commonly accepted mechanism for substrate activation with RMOs, the Mars van Krevelen (MvK) mechanism (Figure 1).[19, 20] In 1954, Mars and van Krevelen published a report detailing the oxidation of organic compounds over vanadium(V) oxide (V_2O_5). In this work, the authors noted that in the presence of heat, organic substrates with weak C-H bonds (e.g. anthracene) could be oxidized by the

[a] Department of Chemistry, University of Rochester, Rochester, NY
E-mail: bpetel@UR.rochester.edu
E-mail: matson@chem.rochester.edu

Dr. Brittney Petel received her bachelor's degree in chemistry at the University of Delaware. She subsequently earned her PhD at the University of Rochester under the supervision of Prof. Ellen Matson. Her thesis focused on the development of vanadium oxide clusters as atomically-precise models for bulk reducible metal oxides. Brittney Petel has earned several awards, including a ACS Women Chemist Committee Travel Award, Eli Huntington Hooker Fellowship and the University of Rochester's Outstanding Graduate Student Award.

Prof. Ellen Matson received her PhD from Purdue University. Following a postdoctoral appointment at the University of Illinois at Urbana-Champaign, Matson began her independent career at the University of Rochester in 2015, where she is currently the Wilmot Assistant Professor of Chemistry. The Matson Laboratory studies the synthesis and reactivity of reduced, organofunctionalized polyoxovanadate clusters. Ellen Matson has earned several awards recognizing early success in research and teaching, including a Sloan Fellowship, Cottrell Scholar Award, Camille Dreyfus Teaching-Scholar Award and the Edith Flanigen Award.

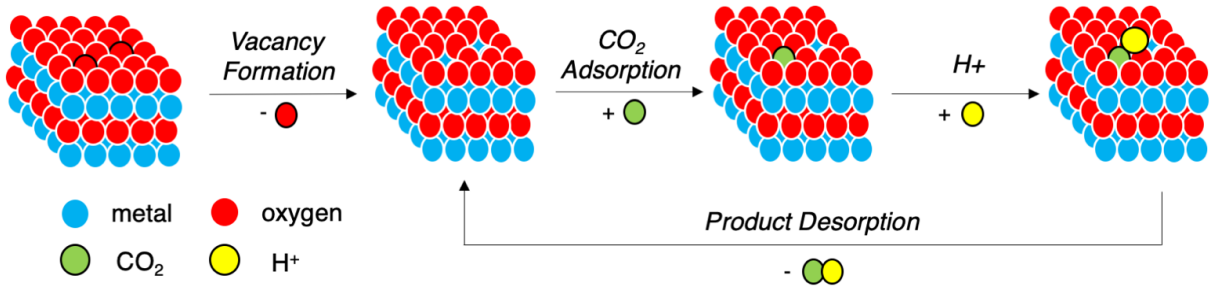

Figure 1. Illustration of the Mars van Krevelen (MvK) mechanism. Key: O, red; transition metal; CO_2, green; H^+, yellow.[19]

material under inert conditions. The authors invoke oxygen atom transfer (OAT) from the RMO to the substrate, resulting in the formation of an oxygen-deficient site at the surface of the material. Subsequent investigations of the reactivity of these oxygen-atom defects revealed that unsaturated metal cations are able to reduce substrates (e.g. O_2, CO_2), resulting in restoration of an oxygen atom at the surface of the material.[19, 21-24]

Certainly, compelling support for the MvK mechanism has been garnered through experimental analysis over the past 60 years.[19, 20, 25-31] However, it is important to note that these investigations provide only indirect evidence of oxygen atom vacancy formation. Difficulties in gaining molecular-level insight into the formation and role of single oxygen vacancies using surface analytical techniques makes the *in situ* identification of these defect sites challenging.[32-38] Thus, to analyze the structural and electronic consequences of creating oxygen-deficient sites on the surface of RMOs during catalysis, researchers have turned to computational investigations, typically involving discreet models (i.e. clusters) to represent small sections of the extended solid.[39-41] These calculations have provided crucial information related to the influence of O-atom removal on the electronics of the RMO. For example, theoretical analysis of the oxidation state of vanadium ions within V_2O_5 show that excess charge, generated via V=O bond cleavage, is redistributed throughout the RMO, ultimately resulting in the reduction of neighboring redox-active metal ions (e.g. $V^{V}_2 \rightarrow V^{III}V^{V}$ (comproportionation) $\rightarrow V^{IV}_2$) .[39-41]

An alternative approach to studying the surface chemistry of metal oxides is through the use homogeneous cluster complexes as molecular models for these materials. In particular, polyoxometalates (POMs) have emerged as promising candidates for modelling extended solids due to their comparable metal oxide surface structure and electronic properties.[42-45] These polynuclear inorganic molecular assemblies are comprised of multiple transition metal oxyanions connected through bridging oxygen atoms, with general formulas of $[M_xO_y]^{n-}$, where M is commonly a high-valent, early-transition metal (e.g. W^{VI}, Mo^{VI}, or V^{V}). One of the most noteworthy characteristics of these polynuclear assemblies is that their composition and delocalized electronic structure often manifests in rich redox properties.[46, 47] Indeed, the electrochemical profile of these polynuclear assemblies have resulted in their applicability in catalysis,[48, 49] nanotechnology,[50, 51] medicine,[52, 53] energy storage,[47, 54-57] and materials science.[49, 58]

Given the similar surface structure and delocalized electronic nature of POMs and metal oxide materials, researchers have targeted an improved understanding of the mechanism of substrate activation at the surface of RMOs via the use of these homogenous cluster complexes. Extensive studies analyzing the oxidation of organic molecules, catalyzed by a Keggin phosphovanadomolybdate cluster (e.g. $[PV_2Mo_{10}O_{40}]^{5-}$), reveals a noteworthy resemblance to the proposed oxidative MvK mechanism. These seminal contributions have revealed that these reactions likely proceed through OAT from the surface of the cluster to the substrate.[59-67] Additional support of a POM-mediated MvK-type mechanism was garnered from theoretical calculations which revealed that the overall free energy of OAT from the heteropolyanion to the organic substrates is energetically favorable (i.e. $\Delta G_{298,Anthrancene}$ = -17.1 kcal/mol).[61] However, to date, isolation and characterization of the expected oxygen-deficient cluster-containing product, complex $[PV_2Mo_{10}O_{39}]^{n-}$, remains elusive.

Indeed, despite the established OAT reactivity of POMs, there is relatively few examples of isolated clusters with surface oxygen-atom defects. This is mainly credited to the difficulties in controlling the metal-to-oxygen ratios within self-assembled POMs, as well as the lack of literature featuring methods for the post-synthetic O-atom abstraction from these discreet metal oxide assemblies. Indeed, "vacancy formation" in POMs has traditionally been relegated to the removal of entire $[MO_x]^n$ subunits (Figure 2, top).[45, 68] Prior to our studies, only a single example of an "oxygen-deficient" POM had been reported; Pope and Pipegrass found that cluster reduction was possible following the proton-assisted reduction of the Keggin ion, $[SiW_{12}O_{40}]^{6-}$.[69, 70] Labelling studies confirmed that these reductive conditions resulted in the conversion of three tungsten (VI)-oxo moieties to three tungsten(IV)-aqua species at the surface of the metal oxide core (Figure 2, bottom).

To further extend our understanding of oxygen atom vacancy formation in POMs, our research group has been investigating defect formation via post synthetic modification of a unique class of these metal oxide assemblies, namely Lindqvist-type polyoxovanadate-alkoxide (POV-alkoxide) clusters ($[V_6O_7(OR)_{12}]^n$; Figure 3).[71-73] Indeed, we have found

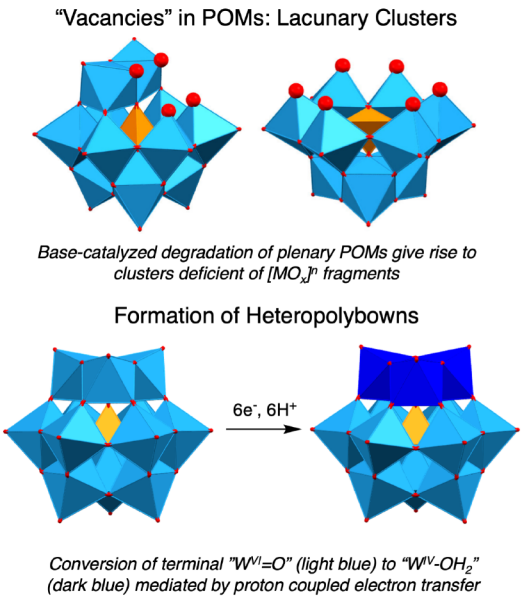

Figure 2. "Vacancies" in polyoxometalate research. Lacunary clusters derived from the addition of base to plenary motifs, pictured are the mono- (top, left) and tri- (top right) lacunary assemblies of the Keggin ion; the vacant site(s) in lacunary structures are highlighted by large spherical oxygen atoms (red). The 6 e^- reduction of the Keggin ion in the presence of acid results in formation of three metal-aqua moieties at the surface of the polyoxotungstate. Light blue polyhedral: W^{VI}; dark blue polyhedral: W^{IV}; red spheres: oxygen; orange polyhedral: Si.[69, 70]

that the structural composition and tunable electronic properties of these alkoxovanadium clusters makes them promising molecular candidates for studying the formation of surface defects in RMOs. These vanadium oxide assemblies have fewer sites available for reduction in comparison to the surface of bulk materials (i.e. only six terminal vanadyl ions, surrounded by inaccessible alkoxide-bridged moieties), presenting a more controlled system that allows for the unambiguous determination of the consequences of removal of a terminal oxido ligand from the surface of the cluster. Furthermore, the bridging alkoxide ligands increase the solubility of these clusters in organic solvents, and provide the opportunity to use homogeneous spectroscopic handles for

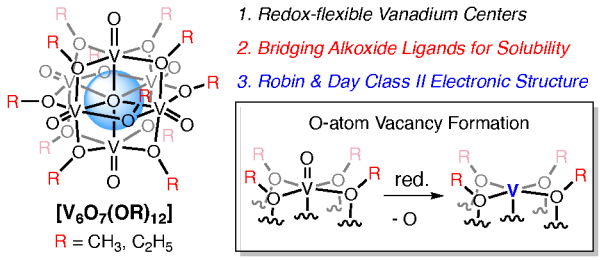

Figure 3. Polyoxovanadate-alkoxide (POV-alkoxide) clusters as models for surface reactivity of metal oxides. Oxygen-atom vacancy formation is observed at vanadyl sites within the Lindqvist assembly upon addition of stochiometric reductant or acid. POV-alkoxide clusters serve as excellent models for this transformations due to their physicochemical properties. Figure reprinted with permission from *Inorg. Chem.* **2019**, *58*, pg. 10462-10471. Copyright 2019 American Chemical Society.

probing defect formation on these model complexes (e.g. ^{1}H NMR spectroscopy).

It is important to note that while there are similarities between POV-alkoxides and bulk vanadium oxide systems, variations in the physical and chemical properties of these clusters and their heterogeneous congeners limits our ability to directly compare the two systems. For example, while the introduction of bridging alkoxide moieties aids in the self-assembly and solubility of our POV-alkoxide clusters, V_xO_y materials typically lack surface ligands.[40, 74] Furthermore, significant variation of the electronic structure of POMs and RMOs (i.e. discreet frontier orbitals and continuum of states, respectively) challenges the ability to electronically compare the clusters and extended solids.[72, 75, 76] Nonetheless, the molecular composition has driven our laboratory to investigate these molecular clusters as models for extended solids.

This feature article summarizes our efforts to understand OAT in polyoxovanadate assemblies, in an attempt to model the surface reactivity of RMOs. Beginning with the initial step of the MvK mechanism (i.e. oxygen atom vacancy generation), we outline synthetic methodologies toward isolating reduced POV-alkoxide clusters via V=O bond cleavage.[77-80] These investigations have resulted in the isolation of a family of oxygen-deficient polyoxometalate clusters, namely $[V_6O_6(OR)_{12}]^n$ (n = -1, 0, 1+; R= CH_3, C_2H_5) and $[V_6O_5(OCH_3)_{12}]^0$. Notably, characterization of the resultant clusters show similar structural and electronic perturbations to that of oxygen deficient vanadium oxides (e.g. V_2O_5, VO_2). Next, a summary of the exploration of these metal oxide surrogates as *functional* models for the extended solids is presented, revealing that the oxygen-deficient clusters are capable of mediating small molecule activation (e.g. O_2 and NO_x^{1-}; x = 2, 3).[77, 81, 82]

Metal Oxygen Bond Cleavage on Lindqvist POV-Alkoxides using V(Mes)$_3$(thf)

Synthesis of Oxygen-deficient Vanadium Oxide Clusters

With the ultimate goal of using POV-alkoxides to analyze the consequence of vacancy formation on metal oxide surfaces, the discovery of synthetic methods to access oxygen deficient vanadium oxide assemblies was required. As such, we began our investigations by targeting vacancy generation on the homometallic, Lindqvist POV-alkoxide cluster, $[V_6O_7(OCH_3)_{12}]^{1-}$.[77] We hypothesized that addition of V(Mes)$_3$(thf) (Mes = 2,4,6-trimethylphenyl), a potent reductant and OAT reagent,[83] to $[V_6O_7(OCH_3)_{12}]^{1-}$ might promote V=O bond cleavage and result in the formation of a cluster bearing a single oxygen-deficient site. Indeed, addition of V(Mes)$_3$(thf) to the fully oxygenated cluster resulted in an immediate color change from green to brown/yellow over the course of 30 minutes (Figure 4, top).

Given the aforementioned solubility of these POV-alkoxides in organic solvents, ^{1}H NMR spectroscopy has proven to be an exceptional tool for analyzing modifications to the cluster surface. The parent, fully-oxygenated cluster has a single, broad resonance located at ~23 ppm in acetonitrile-d_3 (CD_3CN), corresponding to the protons of the twelve, symmetry-

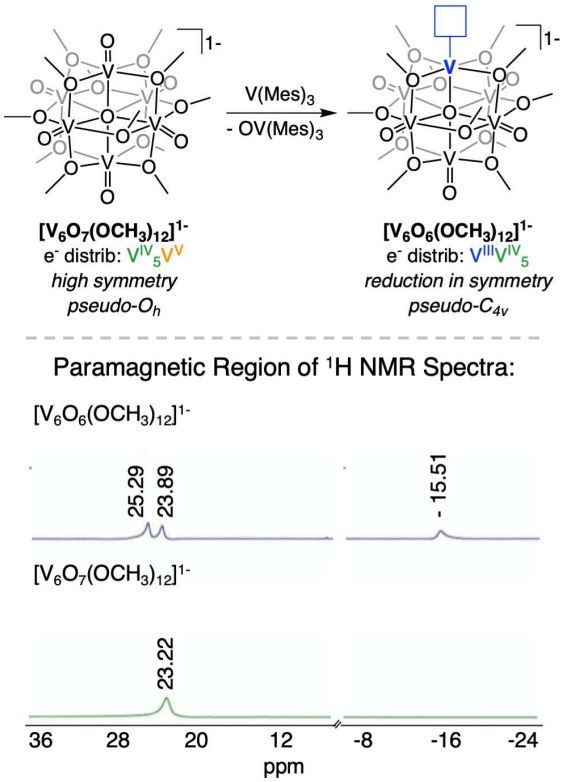

Figure 4. Top, synthesis of oxygen-deficient POV-alkoxide cluster. Bottom, paramagnetic region of ^{1}H NMR spectra of fully-oxygenated POV-alkoxide cluster (bottom, green) and mono-vacant cluster (top, blue) in CD_3CN. Figure reprinted with permission from *J. Am. Chem. Soc.* 2018, **140**, pg. 8424-8428. Copyright 2018 American Chemical Society.

equivalent methoxide ligands of the hexavanadate cluster (Figure 4, bottom). However, removal of a single oxygen atom from the surface of the cluster lowers its symmetry from pseudo-O_h to pseudo-C_{4v}, yielding a spectrum with three resonances (δ (CD_3CN) = 25.3, 23.9, -15.5 ppm). Further analysis of the cluster containing product by electrospray ionization mass spectrometry (ESI-MS; (-)ve mode, carrier solvent: MeOH) revealed formation of a new parent ion with a mass-to-charge ratio (m/z) consistent with the molecular weight of an oxygen-deficient POV-alkoxide cluster, $[V_6O_6(OCH_3)_{12}]^{1-}$, plus an equivalent of methanol.

Characterization of $[V_6O_6(OCH_3)_{12}]^{1-}$ by electronic absorption spectroscopy presented crucial electronic information toward understanding the change in vanadium oxidation state distribution following OAT. The absorption spectra of the mixed-valent parent POV-alkoxide complex (ox. state distribution: $V^{IV}_5V^{V}$) features two intervalence charge transfer (IVCT) bands located 398 nm (ε = 3542 M^{-1} cm^{-1}) and 1000 nm (ε = 814 M^{-1} cm^{-1}); these features are diagnostic of charge transfer between V^{IV} (d^1) and V^{V} (d^0) metal centers within the Lindqvist core.[73] However, following O-atom abstraction, these absorption features disappear, suggesting reduction of the V^{V} ion to V^{III} (ox. state distribution: $V^{III}V^{IV}_5$). Notably, the change in the oxidation state of vanadyl ions within the reduced POV-alkoxide cluster is similar to the theorized electronic consequences of oxygen-atom vacancy formation in V_2O_5.[39-41]

The change in the oxidation state distribution between the parent and mono-vacant clusters (i.e. $V^{V} \rightarrow V^{III}$) suggested that the availability of d^0 vanadyl ions is crucial for the POV-alkoxide to undergo this two-electron redox reaction. Indeed, the reduction of V^{IV} ions embedded within the POV-alkoxide is unlikely as no reports, to date, feature an electron-rich V^{II} ion within a POM. As such, we hypothesized that repeating this reaction with the parent POV-alkoxide cluster in its neutral charge-state, $[V_6O_7(OCH_3)_{12}]^0$ (ox. state distribution: $V^{IV}_4V^{V}_2$), would afford an additional site for OAT, ultimately resulting in the ability to form up to two oxygen vacancies. Through manipulating the equivalence of reductant added [i.e. 1-2 equiv $V(Mes)_3(thf)$], we were able to control the metal-to-oxygen ratio within the cluster, isolating a neutral, mono- and di-vacant POV-alkoxide cluster, $[V_6O_6(OCH_3)_{12}]^0$ ($V^{III}V^{IV}_4V^{V}$) and $[V_6O_5(OCH_3)_{12}]^0$ ($V^{III}_2V^{IV}_4$), respectively (Scheme 2).[79]

Striking changes in the electrochemical profiles of the resultant oxygen-deficient POV-alkoxide clusters were observed via cyclic voltammetry (CV; Figure 5). The CV of the parent, fully-oxygenated Lindqvist POV-alkoxide cluster, $[V_6O_7(OCH_3)_{12}]^0$, features four, quasi-reversible, one-electron redox events, located at +0.83, +0.20, -0.40, and -0.93 V in dichloromethane (vs. $Fc^{0/+}$).[72] These redox processes encompass five redoxmers of the vanadium oxide assembly, ranging from the di-anionic (ox. state distribution: V^{IV}_6) to di-cationic (ox. state distribution: $V^{IV}_2V^{V}_4$) charge-states. However, the CV of the mono-vacant cluster, $[V_6O_6(OCH_3)_{12}]^0$, only possesses three quasi-reversible redox events ($E_{1/2}$ = -0.70, -0.16, and 0.52 V *vs.* $Fc^{0/+}$ in DCM), assigned to sequential oxidation of vanadyl ions. [79] A fourth, irreversible redox event was observed at $E_{p,a}$ = +1.16 V, suggesting that vacancy

Scheme 2. Synthesis of $[V_6O_5(OCH_3)_{12}]^0$ and $V_6O_6(OCH_3)_{12}]^0$.

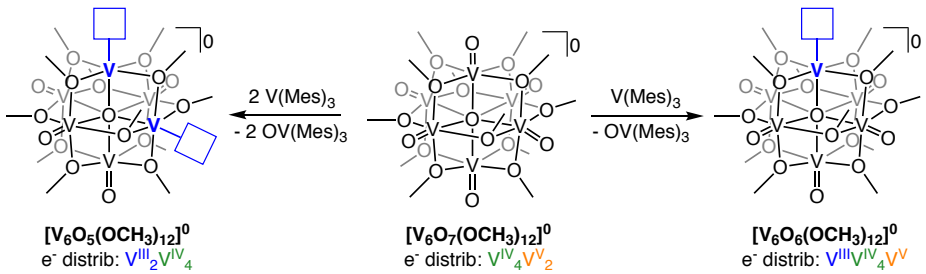

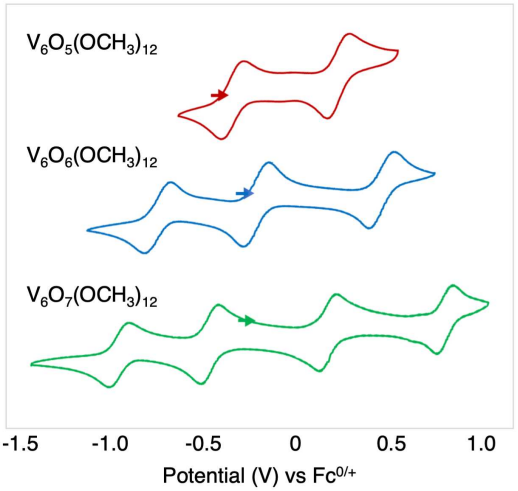

Figure 5. Cyclic voltammograms of fully-oxygenated (bottom, green), mono-vacant (middle, blue), and di-vacant (top, red) POV-alkoxide clusters. CV collected in dichloromethane with 0.1 M $[^nBu_4N][PF_6]$ as supporting electrolyte.[79]

formation translates to oxidative instability of the POV at high potentials.

Similar perturbations were observed in the voltammogram of the di-vacant cluster; in this case, the removal of a second oxygen-atom results in the retention of only two quasi-reversible redox events. We hypothesize that these electronic changes are due to the decoupled nature of the resultant V^{III} ions within the POV-alkoxide, which limits electron transfer to the remaining V^{IV}/V^{V} vanadyl ions within the oxygen-vacant POVs (i.e. only 5 and 4 vanadium ions able to participate in electron transfer in $[V_6O_6(OCH_3)_{12}]^0$ and $[V_6O_5(OCH_3)_{12}]^0$, respectively).

Structural Characterization of Oxygen-deficient POV-alkoxides

With electronic evidence supporting the formation of $[V_6O_6(OCH_3)_{12}]^n$ (n = 1-, 0) and $[V_6O_5(OCH_3)_{12}]^0$ in hand, we next set out to investigate the structural influence of O-atom removal from the POV-alkoxide surface via single-crystal X-ray diffraction (SCXRD; Figure 6, Table 1). In addition to unambiguously confirming the formation of the oxygen-deficient species, SCXRD can provide insight into the structural perturbations that occur across the Lindqvist framework upon defect formation. Furthermore, the growth of crystals with site-differentiated metal ions can provide insight into the valency of the vanadium ions that compose the cluster core via bond valence sum (BVS) calculations.[71, 84] Such investigations would provide atomic-level insight into the structural and electronic consequences of vacancy formation in metal oxides; analyses that accentuate the value of using homogenous inorganic complexes to model heterogenous metal oxides.

To analyze these new oxygen-deficient complexes by SCXRD, we explored crystallization methods toward growing crystals suitable for X-ray analysis.[77] Unfortunately, all crystallization attempts of the monoanionic and neutral, mono-vacant clusters, $[V_6O_6(OCH_3)_{12}]^{1-}$ and $[V_6O_6(OCH_3)_{12}]^0$, respectively, resulted in significant disorder within the unit cell, presenting challenges in performing the desired bond metric analyses. Thus, to modify the mode of crystalization the POV-alkoxide, we oxidized complex $[V_6O_6(OCH_3)_{12}]^{1-}$ with silver triflate, resulting in formation of the triflate-bound POV-alkoxide, $[V_6O_6(OCH_3)_{12}]OTf$. The use of this weakly coordinating anion presented an opportunity to have a large functional group bind to the electron-rich vanadium(III) ion, reducing the overall symmetry of the unit cell. Indeed, crystals that featured site-differentiated vanadyl ions were obtained via cooling methanolic solutions of the cluster to -35 ºC, permitting bond metric analyses.

Significant changes in V-O bond lengths and V-O-V bond angles were observed; removal of a surface oxygen atom resulted in a shortened V1-O_c (O_c = central μ_6-oxygen atom) bond length and truncated V1-O_b-V_n (O_b = bridging methoxide oxygen atom; n = 2, 3, 4, 5) bond angles, relative to that of the parent, fully-oxygenated metal oxide cluster (Figure 6, Table 1).[71] Taken together, these structural variations between the

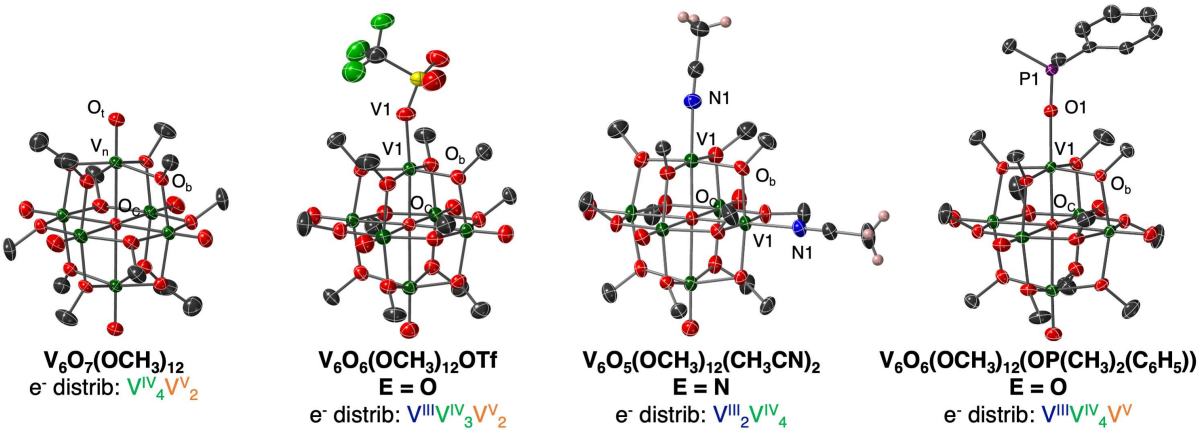

Figure 6. Molecular structures of complexes $[V_6O_7(OCH_3)_{12}]^{1-}$,[71] $[V_6O_6(OCH_3)_{12}]OTf$,[77] $[V_6O_5(OCH_3)_{12}]$,[79] and $[V_6O_6(OCH_3)_{12}(OP(CH_3)_2(C_6H_5)]$[78]. Structures are depicted with 30% probability ellipsoids. Hydrogen atoms, counter ions and solvent molecules have been omitted for clarity. Key: O, red; V, dark green; C, grey; S, yellow; F, light green; N, blue; P, purple; H, pink.

Table 1. Structural parameters of $[V_6O_7(OCH_3)_{12}]^{1-}$,[71] $[V_6O_6(OCH_3)_{12}]OTf$,[77] $[V_6O_5(OCH_3)_{12}]^0$,[79] $[V_6O_6(OCH_3)_{12}(OP(CH_3)_3)]^0$,[78] and $[V_6O_6(OCH_3)_{12}(OP(CH_3)_2(C_6H_5)]^0$.[78]

Bond	Compound				
	$V_6O_7(OCH_3)_{12}^{REF}$	$[V_6O_6(OCH_3)_{12}]OTf^{REF}$ (E = O)	$V_6O_5(OCH_3)_{12}(CH_3CN)_2^{REF}$ (E = N)	$V_6O_6(OCH_3)_{12}(OP(CH_3)_3)^{REF}$ (E = O)	$V_6O_6(OCH_3)_{12}(OP(CH_3)_2(C_6H_5))^{REF}$ (E = O)
V1-E	---	2.052(8) Å	2.112(2) Å, 2.104(3) Å	2.062(5) Å	2.0403(19) Å
V1-O_c	--	2.079(4) Å	2.0666(17) Å, 2.0760(17) Å	2.120(5) Å	2.0982(17) Å
O1-P1	--	--	--	1.467(6) Å	1.5032(19) Å
V1-O_b-V_n	--	105°	105°	105.1°	105.3°
V1-O_b-V1	--	--	96.9°	--	--
V_n-O_c (avg.)	2.25 Å	2.32 Å	2.37 Å	2.31 Å	2.32 Å
V_n-O_t (avg.)	1.60 Å	1.59 Å	1.61 Å	1.59 Å	1.60 Å
V_n-O_b-V_n (avg.)	110°	--	--	--	--

Key: V1= apical V^{III} center; O_c = central μ^6-oxygen atom; O_t = terminal oxygen atom of the vanadyl moieties; V_n = vanadium centers, n= 2-5; O_b = oxygen atom of the bridging methoxide ligands.

parent and oxygen-deficient POV-alkoxides reveal that the reduced vanadium ion is pulled toward the center of the cluster in the oxygen-deficient assemblies.

Similar structural perturbations have been predicted for O-atom removal from the surface of vanadium (V) oxide. Using density functional theory (DFT), Hermann and coworkers found that generation of vacant sites on V_2O_5 results in a substantial reorganization of vanadium ions within the lattice.[39-41] Ultimately, these structural changes are predicted to result in the formation of new V-O-V linkages throughout the extended solid which are hypothesized to stabilize the oxygen-deficient metal oxide. While the geometry of vanadyl ions within vanadium(V) oxide is clearly different from that of the Lindqvist cluster (i.e. V_2O_5, square pyramidal; $V_6O_7(OCH_3)_{12}$, octahedral), the similar movement of the reduced vanadium(III) ion presents further evidence that these vanadium oxide clusters are reasonable models for that of the nanocrystalline material.

Analysis of the molecular structure of the di-vacant species revealed that the two oxygen-deficient sites are located on adjacent vanadium ions within the Lindqvist core (Figure 6).[79] The sole formation of the *cis*-isomer of $[V_6O_5(OCH_3)_{12}]^0$ is likely a result of the structural perturbations observed upon O-atom removal. Similar to the changes observed in bond metric analyses of the triflate-bound species described above, the V^{III} (V1) ions within the di-vacant cluster are pulled toward the central, μ_6-oxygen atom, manifesting in decreased V1-O_c bond lengths and V1-O-V_n bond angles. Indeed, while the *trans*-isomer *could* form following the second O-atom abstraction, the subsequent 0.2 Å truncation of *trans*-V-O_c moieties would result in greater structural perturbations relative to that of the *cis*-vacant molecule, destabilizing the assembly.

With the X-ray data for $[V_6O_6(OCH_3)_{12}]OTf$ and $[V_6O_5(OCH_3)_{12}]^0$ in hand, we next turned our attention to analyzing the oxidation state of vanadyl ions within the hexanuclear core via BVS calculations.[84-86] According to this valence sum rule, the valence of a metal ion can be calculated by summation of the individual bond valences surrounding the atom (Eq 1-2):

$$\text{Valence} = \sum v_{ij} \qquad (1)$$

$$v_{ij} = \left(\frac{R_{ij}}{R_0}\right)^{-N} \qquad (2)$$

where v_{ij} is the individual bond valencies and R_0,[85] b,[84] and N[85] are calculated parameters for the ideal bond length of M^n-E bonds (M^n= metal of 'n' charge state, E= element) and R_{ij} is the experimentally determined bond length(s) in Angstroms (Å). In the case of the vanadium ions in POV-alkoxide clusters, this would be consideration of all V=O_t, V-O_b, and V-O_c bond lengths (O_t = terminal oxo). The BVS calculations of complex $[V_6O_6(OCH_3)_{12}OTf]$ indicate an overall oxidization state distribution of $V^{III}V^{IV}_3V^{V}_2$ (Figure 7).[77] These results not only confirm that O-atom removal results in the two-electron reduction of a V^V ion within the parent POV-alkoxide cluster, but also reveals that the electron-rich V^{III} ion retains its trivalent oxidation state upon oxidation. The retention of the V^{III} ion confirms that the apical vanadium ion is decoupled from the

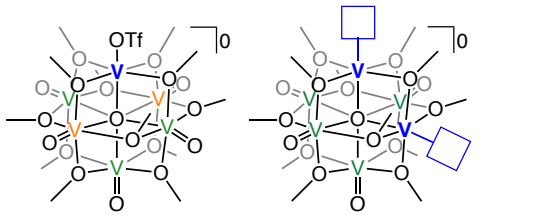

Figure 7. Bond valence sum (BVS) calculations for the crystallographically independent vanadium ions in $[V_6O_6(OCH_3)_{12}]OTf$ (left)[77] and $[V_6O_5(OCH_3)_{12}]^0$ (right)[79]. BVS calculated using equations 1 -2, where R^0 = 1.762 (V^{III}-O), 1.770 (V^{IV}-O) and 1.791 (V^V-O) and b = 0.37. Key: V^{III}, blue; V^{IV}, green; V^V, orange.

remainder of the V=O moieties within the Lindqvist core, as a completely delocalized metal oxide cluster would likely result in comproportionation between V^{V} and V^{III} ions. Notably, DFT calculations describing the electronic perturbations of vacancy generation on V_2O_5 suggest that comproportionation of a V^{V}=O moiety neighboring the reduced V^{III} ion results in the formation of a V^{IV}-O-V^{IV} linkage.[39-41] These results showcase the electronic differences between the Lindqvist cluster and V_2O_5. Similar electronic perturbations were observed in the BVS calculations of the di-vacant complex, which show that the two d^0 vanadyl ions were reduced by two-electrons, resulting in an overall oxidation state distribution of $V^{III}_2V^{IV}_4$.[79]

Alternative Methods for Oxygen-atom Vacancy Formation in POV-alkoxides

Oxygen-atom transfer to tertiary phosphanes

Tertiary phosphanes (PR_3; R = aliphatic, aromatic) have been demonstrated to efficiently remove oxygen atoms from a variety of transition metal-oxo complexes via OAT.[87-94] The prevalent application of phosphanes as oxygen atom acceptors is credited to the strong P=O bond generated following OAT (e.g. $(CH_3)_3PO$; 139 kcal/mol, $(C_6H_5)_3PO$; 127 kcal/mol).[95] As such, we began our efforts toward probing OAT from POV-alkoxide clusters to phosphanes by adding trimethylphosphine ($P(CH_3)_3$) to complex $[V_6O_7(OCH_3)_{12}]^{1-}$. We posed that in analogy to the OAT chemistry observed with $V(Mes)_3(thf)$, OAT to the phosphane would result in the formation of the previously reported oxygen deficient POV-alkoxide cluster. Unfortunately, despite exhaustive modifications to the experimental conditions, no reactivity was observed between the monoanionic, fully-oxygenated cluster and $P(CH_3)_3$. We justified this observation by the fact that the reduced character of the complex requires a more potent reductant for successful OAT. Thus, we turned our attention to the reactivity of $P(CH_3)_3$ with the more-oxidized, neutral POV-alkoxide cluster, $[V_6O_7(OCH_3)_{12}]^0$.[78]

Addition of excess $P(CH_3)_3$ to $[V_6O_7(OCH_3)_{12}]^0$ resulted in complete consumption of the fully-oxygenated cluster after 19 hours at 70 ºC (Figure 8, top). Analysis of the resultant reaction mixture by ^{1}H NMR and electronic absorption did not match that of the previously isolated monovacant cluster.[79] Although the ^{1}H NMR spectra of the product of $[V_6O_7(OCH_3)_{12}]^0$ and $P(CH_3)_3$ was comprised of three paramagnetically shifted and broadened signals, consistent with the expected reduction of cluster symmetry (i.e. *pseudo-*O_h to *pseudo-*C_{4v}), the resonances obtained were shifted from those expected for $[V_6O_6(OCH_3)_{12}]^0$ (Figure 8, bottom). We hypothesized that these inconsistencies were a result of coordination of the byproduct of the reaction, $OP(CH_3)_3$, to the oxygen-deficient site of the reduced POV-alkoxide (i.e. $[V_6O_6(OCH_3)_{12}(OP(CH_3)_3]^0$).

Crystals suitable for SCXRD unambiguously confirmed that the trimethylphosphine oxide byproduct was indeed coordinated to the site-differentiated V^{III} ion (Table 1). Similar to that observed in $[V_6O_6(OCH_3)_{12}]OTf$ and $[V_6O_5(OCH_3)_{12}]^0$, the V1-O_c bond length was decreased by ~0.2 Å. Furthermore, the

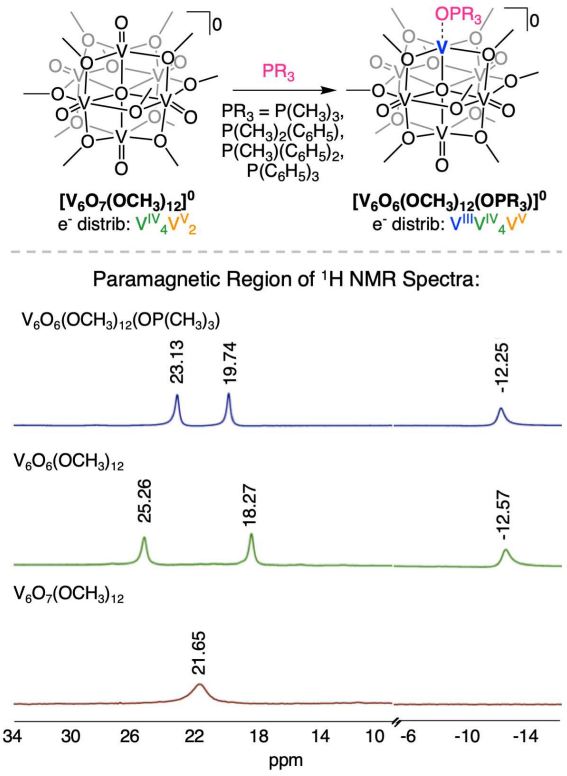

Figure 8. Top, Reduction of POV-methoxide cluster with a series of tertiary phosphanes. Bottom, paramagnetic region of ^{1}H NMR spectra of fully-oxygenated POV-alkoxide cluster (red), mono-vacant cluster (black), and phosphine oxide-bound clusters in CD_3CN.[78]

V1-O1 bond in $[V_6O_6(OCH_3)_{12}(OP(CH_3)_3)]$ was significantly lengthened in comparison to the average V=O_t bond length within the parent cluster.[71] This lengthened V1–O1 bond, coupled to the similar P=O bond distances of free (1.48 Å, theoretically determined[96]) and coordinated (1.467(6) Å) $OP(CH_3)_3$ in complex $[V_6O_6(OCH_3)_{12}(OP(CH_3)_3)]^0$ offered support for a dative interaction between the reduced V^{III} centre and the resultant phosphine oxide moiety. The oxidation state distribution of vanadyl ions within the product was analysed via BVS calculations, revealing the expected mixed-valent distribution for a neutral, oxygen-deficient cluster, $V^{III}V^{IV}_4V^{V}$.

Previous investigations of the influence of phosphane identity on OAT with inorganic metal-oxo complexes have revealed that alteration of the phosphane nucleophilicity and/or cone angle can significantly affect the rate of these reductive transformations.[87, 97-101] To investigate this phenomenon with POV-alkoxide clusters, a series of phosphanes, ranging in nucleophilicity and cone angle (i.e. $P(CH_3)_2(C_6H_5)$, $P(CH_3)(C_6H_5)_2$, $P(C_6H_5)_3$), were added to $[V_6O_7(OCH_3)_{12}]^0$ (Table 2). In each case, phosphine addition resulted in formation of a mono-vacant POV-methoxide cluster with a datively-coordinated phosphine oxide ligand. However, qualitative analysis of the reaction rate showed that the rate of OAT was significantly influenced by the identity of the phosphane. More nucleophilic phosphanes, which also have smaller cone angles, (i.e. $P(CH_3)_3$, $P(CH_3)_2(C_6H_5)$) facilitated OAT

Table 2. Relationship between phosphine nucleophilicity (pKa or an electronic parameter derived from ν(CO) of a nickel compound), cone angle, and reaction time for formation of all (OPR$_3$)-bound clusters.[a]

	$P(CH_3)_3$	$P(CH_3)_2(C_6H_5)$	$P(CH_3)(C_6H_5)_2$	$P(C_6H_5)_3$
pKa [99]	8.65	6.50	4.59	2.73
Electronic parameter [100]	2064.1	2065.3	2067.0	2068.9
Tolman Cone Angle [100]	118	122	136	145
Reaction time $[V_6O_7(OCH_3)_{12}]^0$	19 h	7 h[b]	28 h	15 days
Reaction time $[V_6O_7(OC_2H_5)_{12}]^0$	4 days	4 days	> 20 days	--

[a] General reaction conditions: 1 equiv $[V_6O_7(OCH_3)_{12}]$, 4 equiv phosphane, 70 ºC. [b]only 2 equiv $P(CH_3)_2(C_6H_5)$ used.[78]

in less than 24 h, whereas the larger, less nucleophilic phosphanes, such as $P(C_6H_5)_3$, took significantly longer for complete consumption of $[V_6O_7(OCH_3)_{12}]^0$ (e.g. 15 days; Table 2). These results suggest that the sterics and/or basicity of PR_3 significantly influence OAT from the surface of the cluster.

In an effort to decouple the steric and electronic influences of OAT to PR_3, we extended our investigations to Lindqvist architectures with longer bridging alkoxide ligands. Previously, it has been demonstrated that an increased alkoxide chain length of bridging oxides within the vanadium oxide assembly has no effect on the electronic structure of the hexavanadate core.[72, 76, 102] This suggests that similar OAT between the series of phosphanes and the neutral POV-*ethoxide* cluster, $[V_6O_7(OC_2H_5)_{12}]^0$ (ox. state distribution: $V^{IV}_4V^{V}_2$), would be observed, providing a method to solely examine the correlation between sterics and OAT.

We initiated these efforts by investigating the reactivity of $P(CH_3)_3$ and $P(CH_3)_2(C_6H_5)$ with $[V_6O_7(OC_2H_5)_{12}]^0$.[78] While complete OAT was indeed possible from the POV-ethoxide cluster to the more nucleophilic phosphines, the increased steric bulk surrounding the vanadyl moieties resulted in a 4-fold increase in reaction time in comparison to the POV-methoxide analogues (Table 2). Furthermore, attempts to deoxygenate complex $[V_6O_7(OC_2H_5)_{12}]^0$ with more sterically encumbered phosphanes (i.e. $P(CH_3)(C_6H_5)_2$, $P(C_6H_5)_3$) resulted in limited OAT after prolonged heating (> 2 weeks at 70 ºC).

Acid-induced oxygen-atom vacancy formation

Interested in developing a "green" route for oxygen-atom vacancy formation at the surface of POV-alkoxide clusters, we next turned our attention to the reactivity of $[V_6O_7(OR)_{12}]^n$ with organic acids.[80] Inspiration for these studies was derived from reports describing the electron-proton co-doping mechanism of surface activation of bulk VO_2 (Figure 9).[103, 104] In these reports, formation of low valent vanadium centres were observed upon addition of electrons and protons to the material. While there is debate as to the location of these reduced ions within the material, the authors cite that reduction of the bond order of vanadium oxygen bonds via formation of hydroxyl and aqua ligands within the material.

To model the surface reactivity of VO_2 with acid, we explored stochiometric reactions of our POV-alkoxide cluster in its most-reduced charge state with an organic acid.[80] Following addition of triethylammonium tetrafluoroborate ($[HNEt_3]BF_4$, 1 equiv) to the dianionic POV-ethoxide cluster, $[V_6O_7(OC_2H_5)_{12}]^{2-}$ (1 equiv), analysis of the crude reaction mixture by ^{1}H NMR spectroscopy revealed a series of resonances consistent with the formation of a mixture of products. Signals located at 26.07 and -2.00 ppm correspond to the protons of the bridging ethoxide moieties of the previously reported, monoanionic, POV-ethoxide cluster, $[V_6O_7(OC_2H_5)_{12}]^{1-}$.[76] The remaining paramagnetically shifted and broadened resonances, (δ = 29.56, 28.53, -1.30, -2.56, and -25.66 ppm) suggested formation of an oxygen-deficient organofunctionalized POV cluster, $[V_6O_6(OC_2H_5)_{12}]^{1-}$. The identity of this product was confirmed through independent synthesis of the monoanionic, oxygen-deficient assembly via reduction of the previously reported complex, $[V_6O_6(OC_2H_5)_{12}]^0$.[78]

The formation of an oxygen-deficient metal oxide assembly upon addition of acid is a rare observation in POM chemistry. Studies focused on interactions between POMs and protons typically involve acidification of an aqueous solution containing the polyoxoanion; results have predominantly shown cation exchange processes, yielding metal oxide assemblies with one or more protonated bridging oxido ligands.[105-109] This disparate reactivity of plenary POM motifs is likely due to the fact that these clusters are composed of metal centres with d^0 electronic configurations (e.g. W^{VI}, Mo^{VI}, V^{V}, Ta^{V}, and Nb^{V}). In contrast the

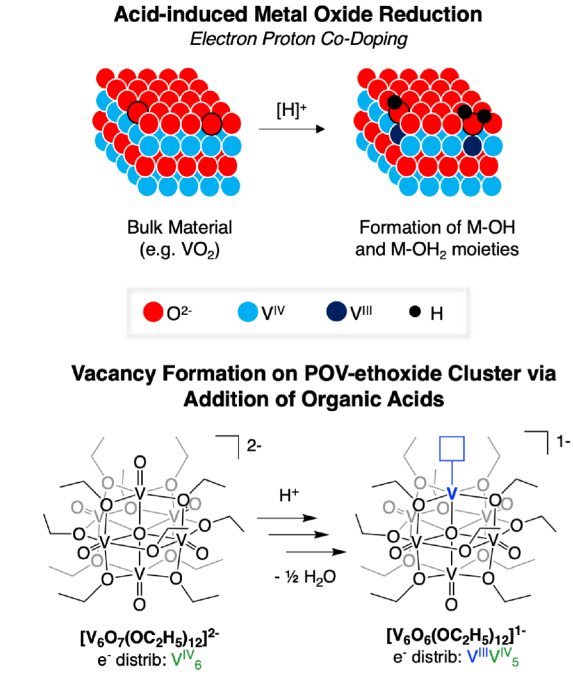

Figure 9. Schematic representation of proton-induced activation on a metal oxide surface (top) and the comparable reactivity observed in POV-alkoxide clusters (bottom).[80]

reduced POV-alkoxide possess six, d^1 V^{IV} ions that provide electron density for proton reduction.

The reactivity of $[V_6O_7(OC_2H_5)_{12}]^{2-}$ with acid more aptly resembles the reported synthesis of reduced, "heteropolybrown" polyoxotungstate architectures, originally reported by Launay and coworkers (Figure 2, bottom).[110-112] In this study, the authors propose that the six-electron reduction of the polyoxotungstate Keggin ion, $[(H_2)W_{12}O_{40}]^{6-}$, via controlled potential electrolysis under acidic conditions, results in the reduction of three terminal W^{VI}=O moieties to W^{IV}-OH_2 groups.[69] In a subsequent article, Piepgrass and Pope spectroscopically confirm the proposed structural configuration.[113]

Small Molecule Activation by Oxygen-deficient POV-alkoxides

Computational investigations on RMO-catalyzed OAT processes have determined that substrate-surface interactions can enable the formation of deoxygenated products though multi-electron redox reactions at defect sites within bulk materials.[24] However, challenges in monitoring reaction progress using current *in situ* or *in operando* analytical techniques have hampered our understanding of the structural and electronic perturbations of RMO surfaces during heterogeneous OAT transformations.[32-38] As such, with the aforementioned strategies in hand for oxygen-atom removal from the surface of POV-alkoxide clusters, we turned our attention to the reactivity of the defect sites in these molecular assemblies. In this section, we explore the mediation of small molecule (e.g. O_2,[77] NO_x^{1-}; x = 2, 3[81, 82]) activation with oxygen-deficient POV-alkoxide clusters. Overall, the capability of the mono-vacant POV-alkoxide clusters to facilitate substrate coordination and activation confirms that Lindqvist metal oxide cluster complexes can serve as a functional model for RMO-catalyzed MvK transformations.

Dioxygen reduction with oxygen-deficient POV-alkoxide clusters

The reduction of O_2 is an important step in heterogenous catalysis.[114, 115] Indeed, the addition of molecular oxygen to extended solids can influence both the chemical composition and reactivity of the solid support. For example, surface-O_2 interactions are crucial in a wide variety of industrially important transformations such as chemical conversion (i.e. CO and hydrocarbon conversion)[116-119] and electrocatalysis (i.e. oxygen reduction reaction in fuel cells).[120-122] Furthermore, molecular oxygen is typically added to reduced RMOs to restore surface oxygen atoms via oxygen exchange between the solid support and gaseous reactant.[19, 21-23] This process makes RMO materials recyclable, often remaining operational for several years.[16, 123, 124]

Given the importance of O_2 interactions with RMOs, we decided to begin our investigations into the reactivity of oxygen-deficient POV-alkoxide clusters with O_2. Addition of 1 atm of O_2 to $[V_6O_6(OCH_3)_{12}]^{1-}$ resulted in quantitative formation of the fully-oxygenated cluster, $[V_6O_7(OCH_3)_{12}]^{1-}$, after 24 hours at 50 ºC (Scheme 3). To probe the solution stability of the monovacant cluster at the relevant reaction conditions, a control experiment was conducted by heating $[V_6O_6(OCH_3)_{12}]^{1-}$ to 50 ºC for 24 hours; no evidence of cluster degradation was observed. Furthermore, confirmation that the oxygen-atom participating in OAT was from O_2 reduction was achieved via the addition of isotopically-enriched dioxygen ($^{18}O_2$). Analysis of the resulting product by ^{1}H NMR and electrospray ionization mass-spectrometry (ESI-MS) confirmed formation of the corresponding labelled product, $[V_6O_6{}^{18}O(OCH_3)_{12}]^{1-}$ (Figure 10, bottom). Collectively, these results confirm that the oxygen-deficient cluster can reduce molecular oxygen, revealing the propensity of the surface-defect on the homogenous molecular model to facilitate activation of oxygenated substrates.

Scheme 3. Reactivity of $[V_6O_6(OCH_3)_{12}]^{1-}$ with O_2.

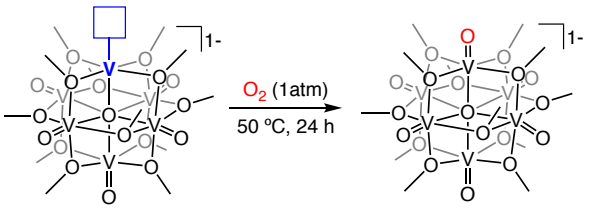

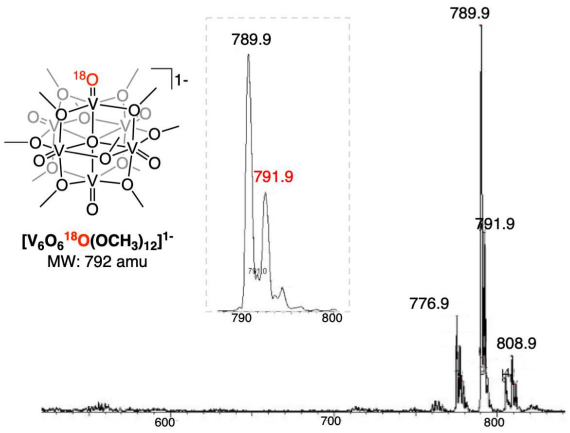

Figure 10. ESI-MS (-)ve mode of control experiment using $^{18}O_2$ (1 atm). Inset highlights mass distribution resulting from incorporation of labelled oxygen atoms within the hexavanadate cluster (red), however the un-labelled cluster ($[V_6O_7(OCH_3)_{12}]^{1-}$; *m/z* 790), is observed in a relatively high quantity. This is likely due to exchange of H_2O with $[V_6O_6{}^{18}O(OCH_3)_{12}]^{1-}$. Figure reprinted with permission from *J. Am. Chem. Soc.* 2018, **140**, pg. 8424-8428. Copyright 2018 American Chemical Society.

Reduction of nitrogen-containing oxyanions with oxygen-deficient POV-alkoxide clusters

To expand the reactivity profile of the mono-vacant POV-alkoxide cluster, we became interested in investigating whether $[V_6O_6(OCH_3)_{12}]^{1-}$ could mediate the reduction of oxyanions, specifically nitrite (NO_2^{1-}; one-electron reduction) and nitrate (NO_3^{1-}; two-electron reduction). Although POMs are well-established to facilitate the electrocatalytic reduction of these oxyanions,[47] it is unclear how these oxide-terminated polyoxoanions bind to the substrate and facilitate the requisite

Scheme 4. Reactivity of $[V_6O_6(OCH_3)_{12}]^{1-}$ with NO_2^{1-} (left) and NO_3^{1-} (right).[81]

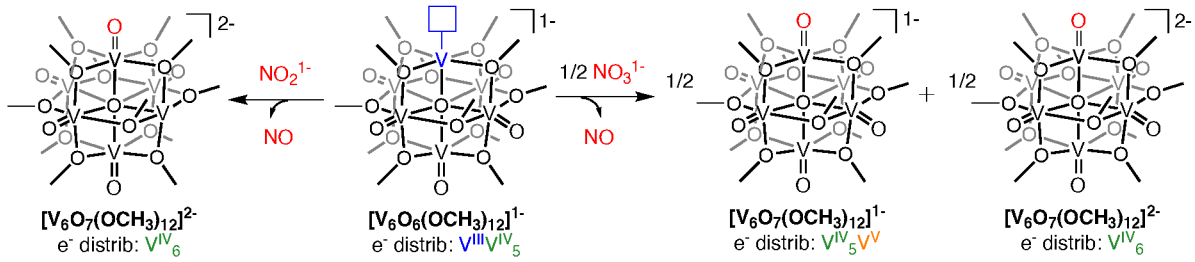

OAT chemistry. In cases where mechanistic insight has been presented, these transformations are commonly mediated by transition metal-substituted polyoxoanions, where substrate activation occurs at the heterometallic center.[47, 125-128]

Addition of 1 equiv of NO_2^{1-} to complex $[V_6O_6(OCH_3)_{12}]^{1-}$ resulted in the one-electron reduction of NO_2^{1-} and OAT to the reduced POV-alkoxide.[81] This translated to the release of nitric oxide (NO), and formation of the dianionic POV-alkoxide cluster, $[V_6O_7(OCH_3)_{12}]^{2-}$ (Scheme 4). Formation of the fully-oxygenated cluster in its most reduced charge state was confirmed via electronic absorption spectroscopy; the lack of IVCT bands attributed to mixed-valent POV-alkoxides is consistent with the formation of the $[V^{IV}_6]^{2-}$ cluster.[73] Confirmation of N-O bond scission was garnered from NO-trapping experiments using cobalt tetraphenylporphyrin (CoTPP).[129-132]

We next set out to explore if the oxygen-deficient POV-alkoxide would be able to mediate the two-electron reduction of NO_3^{1-}. While this transformation is significantly more endergonic than that of nitrite reduction,[133, 134] we hypothesized that NO_3^{1-} activation would follow a similar pathway; following coordination of NO_3^{1-} to the oxygen deficient POV-alkoxide, two electrons would be transferred to the substrate resulting in N-O bond cleavage (formation of NO_2^{1-}). In this case, the expected reactivity would result in a change in the overall oxidation state distribution of the cluster from $[V^{III}V^{IV}_5]^{1-}$ to $[V^{IV}_5V^{V}]^{1-}$ (i.e. $[V_6O_7(OCH_3)_{12}]^{1-}$). Although addition of $[^nBu_4N]NO_3$ to $[V_6O_6(OCH_3)_{12}]^{1-}$ at 21 °C resulted in only minimal conversion to product, heating the reaction to 70 ºC resulted in complete conversion of the oxygen-deficient cluster.

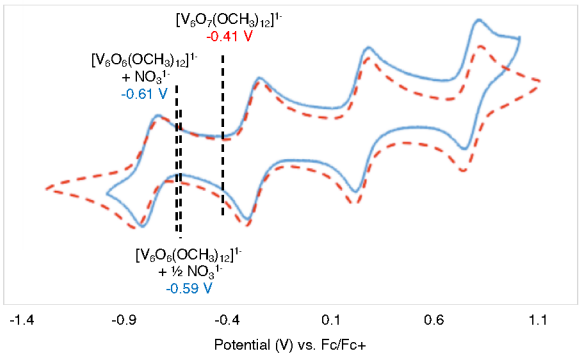

Figure 11. Open circuit potential for the independently synthesized, fully-oxygenated cluster ($[V_6O_6(OCH_3)_{12}]^{1-}$; -0.41V, red) and the products of NO_3^{1-} reduction (stoichiometric, -0.61V; sub-stoichiometric, -0.59 V) via $[V_6O_6(OCH_3)_{12}]^{1-}$. CV collected in acetonitrile with 0.1 M $[^nBu_4N][PF_6]$ as supporting electrolyte.[81]

Further analysis of the resulting cluster-containing product by electronic absorption spectroscopy and cyclic voltammetry showed substantial inconsistencies from that which would be expected for the monoanionic POV-alkoxide cluster, $[V_6O_7(OCH_3)_{12}]^1$ (Figure 11). For example, the absorption spectrum of the crude product contains two IVCT bands located at 392 nm (2594 M^{-1} cm^{-1}) and 1000 nm (605 M^{-1} cm^{-1}), consistent with formation of a cluster with a mixed-valent $V^{IV/V}$ oxidation state distribution. However, comparison of the molar absorptivity values between the nitrate reduction product and that of the independently synthesized monoanionic cluster, $[V_6O_7(OCH_3)_{12}]^{1-}$,[73] revealed that the IVCT intensities are significantly lower than expected. These results, coupled with an open circuit potential for the product shifted cathodically by 0.2 V (Figure 11), suggested that complex $[V_6O_7(OCH_3)_{12}]^{1-}$ is not the sole product of this reaction.

Given that NO_2^{1-} reduction occurs at room temperature, we hypothesized that the nitrogen-containing byproduct of nitrate reduction, NO_2^{1-}, could be competing with the two-electron reduction of NO_3^{1-}; following deoxygenation of NO_3^{1-}, unreacted starting material ($[V_6O_6(OCH_3)_{12}]^{1-}$) would preferentially reduce the *in situ* generated NO_2^{1-}, resulting in the formation of the dianionic POV-alkoxide cluster, $[V_6O_7(OCH_3)_{12}]^{2-}$. To test this hypothesis, a substiochiometric amount of $[^nBu_4N]NO_3$ (0.5 equiv) was added to $[V_6O_6(OCH_3)_{12}]^{1-}$. Analysis of the resulting product by ^1H NMR revealed that although only half of the required substrate was added, complete conversion of the oxygen-deficient cluster was observed (Scheme 4). Further analysis of the cluster-containing products in the substiochiometric reaction, via cyclic voltammetry, confirm that the same ratio of POV-alkoxide clusters are formed regardless of NO_2^{1-} equivalence (Figure 11).

To analyze both the effect of changing the surface structure and oxidation state distribution of the Lindqvist cluster, we opted to investigate the reactivity of the redox-series of monovacant POV-ethoxide clusters, $[V_6O_6(OC_2H_5)_{12}]^n$ (n = 1-, 0, 1+) with NO_x^{1-} (x = 2, 3).[82] Spectroscopic investigations of the POV-ethoxides have revealed that the site-differentiated vanadium(III) centre retains its oxidation state across all three charge states of the cluster,[78, 80, 135] providing a method for analysing the influence of the oxidation state of remote vanadyl ions (i.e. cluster redox potential) on N-O bond scission. Furthermore, alteration of the bridging alkoxide chain length,

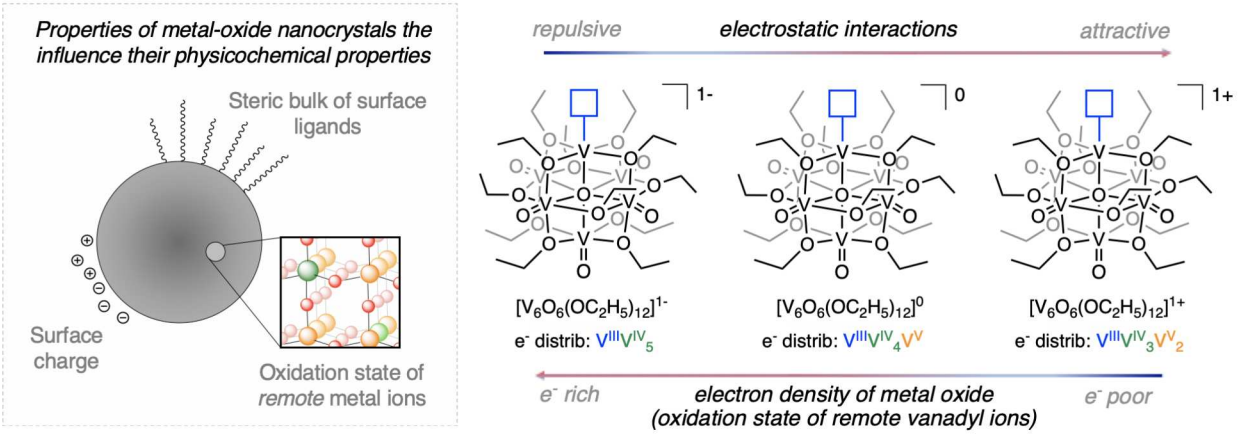

Figure 12. Physicochemical properties that influence the reactivity of metal oxides, including chemical composition of surface ligands, surface charge, and the oxidation state of remote metal ions surrounding the catalytically active metal center (left). Key: red, O; green, V.; orange, remote vanadyl ions. Structure-function investigations reveal the role these properties play in dictating the rate of oxyanion reduction at the surface of oxygen-deficient POV-alkoxide clusters. Figure is reprinted, in part, with permission from *Inorg. Chem.* (DOI: 10.1021/acs.inorgchem.0c02052). Copyright 2020 American Chemical Society.

from methoxide to ethoxide, presents the opportunity to concurrently analyse the effect of changing the steric accessibility of the active V^{III} ion on reaction rate.

Collectively, these investigations revealed that NO_x^{1-} reduction is influenced by three factors. As expected, both the ligand identity (i.e. Table 3, entry 1 vs 2) and oxidation state distribution of neighbouring vanadyl moieties (i.e. Table 3, entry 2-4) significantly influence the rate of NO_x^{1-} activation, with OAT reaction times ranging from 5 minutes to 96 hours. Furthermore, our investigations revealed that ion-pairing interactions, in particular, repulsive substrate-cluster interactions, hinder the rate of OAT for both nitrite and nitrate reduction (Table 3, entry 2 vs. entries 3-4). We anticipate that similar consequences might be observed in the analogous reduction chemistries with heterogenous systems. These factors reveal design strategies that could improve the OAT reactivity of metal oxides, ultimately resulting in the synthesis of new, efficient heterogeneous catalysts for the activation of oxyanions.

Table 3. Comparative reaction times and temperatures for NO_x^{1-} (x = 2, 3) reduction via $[V_6O_6(OCH_3)_{12}]^{1-}$ and the redox-series of POV-*ethoxide* clusters. Table is reprinted, in part, with permission from *Inorg. Chem.* (DOI: 10.1021/acs.inorgchem.0c02052). Copyright 2020 American Chemical Society.

	Complex	Ox. State Distrib.	NO_2^{1-} Reduction Conditions	NO_3^{1-} Reduction Conditions
1	$[V_6O_6(OCH_3)_{12}]^{1-}$	$V^{III}V^{IV}_5$	24 h, 21 °C	24 h, 70 °C
2	$[V_6O_6(OC_2H_5)_{12}]^{1-}$	$V^{III}V^{IV}_5$	30 min, 21 °C	24 h, 50 °C
3	$[V_6O_6(OC_2H_5)_{12}]^{0}$	$V^{III}V^{IV}_4V^{V}$	5 min, 21 °C	1.5 h, 50 °C
4	$[V_6O_6(OC_2H_5)_{12}]^{1+}$	$V^{III}V^{IV}_3V^{V}_2$	15 min, 21 °C	96 h, 50 °C

Conclusions and Outlook

In summary, over the past four years we have investigated Lindqvist POV-alkoxide clusters as atomically-precise analogues of vanadium oxide materials, with particular interest in studying defect formation in RMOs. Driven by our ultimate goal of gaining a molecular-level insight into the structural and electronic perturbations of metal oxide supports during catalysis (i.e. the MvK mechanism; vacancy formation, substrate adsorption, substrate activation, product desorption), we began by developing new methods for the post-synthetic removal of oxygen-atoms from terminal vanadyl ions within the cluster core. Indeed, addition of reductants (e.g. $V(Mes)_3(thf)$ or PR_3) or acid to the fully-oxygenated vanadium oxide clusters resulted in the generation of a redox-series of oxygen-deficient POV-alkoxide clusters that feature up to two coordinatively unsaturated vanadium ions. Rigorous electronic characterization of the mono- and di-vacant clusters revealed that O-atom removal results in the formation of V^{III} moieties as site-differentiated ions that are decoupled from the remaining Robin and Day Class II delocalized cluster core. In addition, structural characterization, via SCXRD, revealed that O-atom removal results in significant lattice distortions; the reduced vanadium ion(s) is pulled toward the centre of the cluster, resulting in a ~0.2 Å truncation of the V-O_c bond.

We have also analysed the reactivity of the reduced POV-alkoxides by investigating transformations relevant to the reduction of chemical pollutants and other oxygenated substrates. While not described herein, we have also demonstrated that the oxygen-deficient POV-alkoxides can mediate the deoxygenation of organic substrates, such as the conversion of styrene oxide to styrene . In all cases, substrate reduction and OAT results in restoration of an oxygen atom to the site-differentiated V^{III} ion. Analysis of reaction parameters that influence substrate reduction revealed that OAT is influenced by the sterics of the alkoxide ligands surrounding the active V^{III} ion, substrate-cluster electrostatic interactions, and cluster charge state or redox potential. Collectively, these investigations have revealed that polyoxometalates can serve not only as structural and electronic models for reduced RMOs

but also provide a method for modelling heterogenous OAT processes that invoke the MvK mechanism.

Looking forward, the ability to further expand Lindqvist POV-alkoxide clusters as atomically-precise models for metal oxides is promising, given the recently developed syntheses of heterometal-functionalized POV-alkoxide clusters, e.g. $[V_{6-x}O_{7-x}(OCH_3)_{12}(MX')_x]$ (x =1 , MX' = FeOTf,[136] FeCl,[137] GaCl,[137] $Ti(OCH_3)$,[138] $Hr(OCH_3)$,[138] $Zr(OCH_3)$; x = 2, MX' = $Ti(OCH_3)$).[139] These multimetallic clusters can serve as structural and electronic models for cationically doped transition metal oxides which are commonly used as catalysts in industrially relevant transformations.[15] Indeed, it is well established that the chemical and photochemical behavior of a metal oxide can be modified by introducing heterometallic dopants. Ideally, analyzing vacancy generation on $[V_{6-x}O_{7-x}(OCH_3)_{12}(MX')_x]$ will provide atomistic insight into the consequences of dopant addition on the MvK reactivity of metal oxides. In particular, we are interested in investigating the relative ability to mediate V=O bond cleavage on the heterometallic systems, the location of the resulting unsaturated vanadyl ion (i.e. *cis*- vs *trans*- to the heterometal), as well as the influence of the heterometal on substrate deoxygenation. Ultimately, insights from this work will reveal important design considerations for the generation of ternary metal oxides as heterogeneous catalysts for small molecule activation and chemical valorization.

Conflicts of interest

There are no conflicts to declare.

Acknowledgements

The authors gratefully acknowledge support for this research from the National Science Foundation (CHE-1653195) and from the University of Rochester. E. M. M. is a recipient of a Cottrell Scholar award from the Research Corporation for Science Advancement which has also financially contributed to support this work. The authors acknowledge acknowledge William W. Brennessel and the X-ray Crystallographic Facility of the Department of Chemistry at the University of Rochester for SCXRD analysis. Dr. Thomas Auvray is acknowledged for assistance in the preparation of Figure 2. The authors would also like to acknowledge Alex A. Fertig, Michela L. Maiola, Rachel L. Meyer, and Eric Schreiber, for assistance with data collection and interpretation of results during the investigations described hererin.

Notes and references

1. *Metal Oxides: Chemistry and Applications*, Taylor & Francis Group, Boca Raton, Fl, 2006.
2. A. Ruiz Puigdollers, P. Schlexer, S. Tosoni and G. Pacchioni, *ACS Catalysis*, 2017, **7**, 6493-6513.
3. J. C. Vedrine, *Metal Oxides in Heterogeneous Catalysis*, Elsevier, Saint Louis, UNITED STATES, 2018.
4. C. Yuan, H. B. Wu, Y. Xie and X. W. Lou, *Angewandte Chemie International Edition*, 2014, **53**, 1488-1504.
5. X. Yu, T. J. Marks and A. Facchetti, *Nature Materials*, 2016, **15**, 383-396.
6. X. Xia, Y. Zhang, D. Chao, C. Guan, Y. Zhang, L. Li, X. Ge, I. M. Bacho, J. Tu and H. J. Fan, *Nanoscale*, 2014, **6**, 5008-5048.
7. J. C. Védrine, *Catalysts*, 2017, **7**, 341-366.
8. T. N. Pham, T. Sooknoi, S. P. Crossley and D. E. Resasco, *ACS Catalysis*, 2013, **3**, 2456-2473.
9. M. Hara, K. Nakajima and K. Kamata, *Science and Technology of Advanced Materials*, 2015, **16**, 034903.
10. P. Schwach, X. Pan and X. Bao, *Chemical Reviews*, 2017, **117**, 8497-8520.
11. H. Chen, C. E. Nanayakkara and V. H. Grassian, *Chemical Reviews*, 2012, **112**, 5919-5948.
12. X. Jiang, X. Nie, X. Guo, C. Song and J. G. Chen, *Chemical Reviews*, 2020, DOI: 10.1021/acs.chemrev.9b00723.
13. S. Dang, H. Yang, P. Gao, H. Wang, X. Li, W. Wei and Y. Sun, *Catalysis Today*, 2019, **330**, 61-75.
14. R.-P. Ye, J. Ding, W. Gong, M. D. Argyle, Q. Zhong, Y. Wang, C. K. Russell, Z. Xu, A. G. Russell, Q. Li, M. Fan and Y.-G. Yao, *Nature Communications*, 2019, **10**, 5698.
15. E. W. McFarland and H. Metiu, *Chem Rev*, 2013, **113**, 4391-4427.
16. J. A. H. Dumesic, G.W.; Boudart, M., *Handbook of Heterogeneous Catalysis*, ed. H. K. G. Ertl, F. Schüth and J. Weitkamp, 2008.
17. J. Jia, C. Qian, Y. Dong, Y. F. Li, H. Wang, M. Ghoussoub, K. T. Butler, A. Walsh and G. A. Ozin, *Chemical Society Reviews*, 2017, **46**, 4631-4644.
18. P. L. Gai-Boyes, *Catalysis Reviews*, 1992, **34**, 1-54.
19. P. Mars and D. W. van Krevelen, *Chemical Engineering Science*, 1954, **3**, 41-59.
20. C. Doornkamp and V. Ponec, *Journal of Molecular Catalysis A: Chemical*, 2000, **162**, 19-32.
21. P. Schlexer, D. Widmann, R. J. Behm and G. Pacchioni, *ACS Catalysis*, 2018, **8**, 6513-6525.
22. M. A. Henderson, W. S. Epling, C. L. Perkins, C. H. F. Peden and U. Diebold, *The Journal of Physical Chemistry B*, 1999, **103**, 5328-5337.
23. A. R. Almeida, J. A. Moulijn and G. Mul, *The Journal of Physical Chemistry C*, 2011, **115**, 1330-1338.
24. N. Kumari, M. A. Haider, M. Agarwal, N. Sinha and S. Basu, *The Journal of Physical Chemistry C*, 2016, **120**, 16626-16635.
25. C. E. Senseman and O. A. Nelson, *Industrial & Engineering Chemistry*, 1923, **15**, 521-524.
26. W. i. K. Schreiber, M., , *Grenzflachen-Katalyse*, Leipzig, 1933.
27. C. R. D. J.M. Weiss, R.M. Burns *Ind. Eng. Chem.*, 1923, **15**, 005.
28. E. B. Maxted, *J. Soc. Chem. Ind.*, 1928, **47**, 101.
29. P. H. Calderbank, *The Indust. Chemist*, 1952, 201.
30. C. Doornkamp, M. Clement and V. Ponec, *Applied Catalysis A: General*, 1999, **188**, 325-336.
31. A. V. Mironenko and D. G. Vlachos, *Journal of the American Chemical Society*, 2016, **138**, 8104-8113.
32. L. J. Lauhon and W. Ho, *Rev Sci Instrum*, 2001, **72**, 216-223.
33. C. Bai, *Scanning Tunneling Microscopy and Its Application*, Shenghai Scientific & Technical Publishers, China, 2nd, Revised Edition edn., 2000.
34. R. V. Lapshin, *Meas Sci Technol*, 2007, **18**, 907-927.

35. F. Marinello, M. Balcon, P. Schiavuta, S. Carmignato and E. Savio, *Meas Sci Technol*, 2011, **22**, 1-9.
36. U. Diebold, *Surf Sci Rep*, 2003, **48**, 53-229.
37. F. Gołek, P. Mazur, Z. Ryszka and S. Zuber, *Applied Surface Science*, 2014, **304**, 11-19.
38. M. Ek, Q. M. Ramasse, L. Arnarson, P. Georg Moses and S. Helveg, *Nat Commun*, 2017, **8**, 1-9.
39. K. Hermann, M. Witko, R. Druzinic and R. Tokarz, *Applied Physics A*, 2001, **72**, 429-442.
40. A. Michalak, M. Witko and K. Hermann, *Surface Science*, 1997, **375**, 385-394.
41. K. Hermann, M. Witko and R. Druzinic, *Faraday Discussions*, 1999, **114**, 53-66.
42. M. T. Pope, Muller, A., *Polyoxometalate Chemistry: From Topology via Self-Assembly to Applications.* Berlin, 2001.
43. N. I. Gumerova and A. Rompel, *Nature Reviews Chemistry*, 2018, **2**, 0112.
44. X. C. Lopez, J. J.; Bo, C.; Poblet, J. M., *Chem. Soc. Rev.* , 2012, **41**, 7537-7571.
45. P. Gouzerh and A. Proust, *Chemical Reviews*, 1998, **98**, 77-112.
46. T. Ueda, *ChemElectroChem*, 2018, **5**, 823-838.
47. M. Sadakane and E. Steckhan, *Chemical Reviews*, 1998, **98**, 219-238.
48. J.-J. Ye and C.-D. Wu, *Dalton Transactions*, 2016, **45**, 10101-10112.
49. D. C. C. Soumyajit Roy, and Tatjana N. Parac-Vogt, *Editorial: Polyoxometalates in Catalysis, Biology, Energy and Materials Science*, 2019.
50. D.-L. Long, R. Tsunashima and L. Cronin, *Angewandte Chemie International Edition*, 2010, **49**, 1736-1758.
51. F. F. Bamoharram, *Synthesis and Reactivity in Inorganic, Metal-Organic, and Nano-Metal Chemistry*, 2011, **41**, 893-922.
52. J. T. Rhule, C. L. Hill, D. A. Judd and R. F. Schinazi, *Chemical Reviews*, 1998, **98**, 327-358.
53. T. Yamase, in *Biomedical Inorganic Polymers: Bioactivity and Applications of Natural and Synthetic Polymeric Inorganic Molecules*, eds. W. E. G. Müller, X. Wang and H. C. Schröder, Springer Berlin Heidelberg, Berlin, Heidelberg, 2013, 65-116.
54. M. Genovese and K. Lian, *Current Opinion in Solid State and Materials Science*, 2015, **19**, 126-137.
55. H. D. Pratt, N. S. Hudak, X. Fang and T. M. Anderson, *Journal of Power Sources*, 2013, **236**, 259-264.
56. H. D. Pratt, W. R. Pratt, X. Fang, N. S. Hudak and T. M. Anderson, *Electrochimica Acta*, 2014, **138**, 210-214.
57. L. E. VanGelder, T. R. Cook and E. M. Matson, *Comments on Inorganic Chemistry*, 2019, **39**, 51-89.
58. M. Samaniyan, M. Mirzaei, R. Khajavian, H. Eshtiagh-Hosseini and C. Streb, *ACS Catalysis*, 2019, **9**, 10174-10191.
59. A. M. Khenkin, L. Weiner, Y. Wang and R. Neumann, *Journal of the American Chemical Society*, 2001, **123**, 8531-8542.
60. A. M. Khenkin and R. Neumann, *Angewandte Chemie International Edition*, 2000, **39**, 4088-4090.
61. I. Efremenko and R. Neumann, *Journal of the American Chemical Society*, 2012, **134**, 20669-20680.
62. A. M. Khenkin, G. Leitus and R. Neumann, *Journal of the American Chemical Society*, 2010, **132**, 11446-11448.
63. R. Neumann and A. M. Khenkin, *Chemical Communications*, 2006, **24**, 2529-2538.
64. A. M. Khenkin and R. Neumann, *Journal of the American Chemical Society*, 2008, **130**, 14474-14476.
65. H. Goldberg, I. Kaminker, D. Goldfarb and R. Neumann, *Inorganic Chemistry*, 2009, **48**, 7947-7952.
66. B. B. Sarma, R. Carmieli, A. Collauto, I. Efremenko, J. M. L. Martin and R. Neumann, *ACS Catalysis*, 2016, **6**, 6403-6407.
67. B. B. Sarma, I. Efremenko and R. Neumann, *Journal of the American Chemical Society*, 2015, **137**, 5916-5922.
68. T. Minato, K. Suzuki, K. Yamaguchi and N. Mizuno, *Chemistry – A European Journal*, 2017, **23**, 14213-14220.
69. K. Piepgrass and M. T. Pope, *Journal of the American Chemical Society*, 1987, **109**, 1586-1587.
70. K. Piepgrass and M. T. Pope, *Journal of the American Chemical Society*, 1989, **111**, 753-754.
71. C. D. Johann Spandl, Irene Brüdgam, Hans Hartl, *Angewandte Chemie International Edition*, 2003, **42**, 1163-1166.
72. C. Daniel and H. Hartl, *Journal of the American Chemical Society*, 2005, **127**, 13978-13987.
73. C. Daniel and H. Hartl, *Journal of the American Chemical Society*, 2009, **131**, 5101-5114.
74. S. Surnev, M. G. Ramsey and F. P. Netzer, *Progress in Surface Science*, 2003, **73**, 117-165.
75. A. Walsh and K. T. Butler, *Accounts of Chemical Research*, 2014, **47**, 364-372.
76. L. E. VanGelder, A. M. Kosswattaarachchi, P. L. Forrestel, T. R. Cook and E. M. Matson, *Chemical Science*, 2018, **9**, 1692-1699.
77. B. E. Petel, W. W. Brennessel and E. M. Matson, *J Am Chem Soc*, 2018, **140**, 8424-8428.
78. B. E. Petel, R. L. Meyer, W. W. Brennessel and E. M. Matson, *Chemical Science*, 2019, **10**, 8035-8045.
79. B. E. Petel, A. A. Fertig, M. L. Maiola, W. W. Brennessel and E. M. Matson, *Inorganic Chemistry*, 2019, **58**, 10462-10471.
80. E. Schreiber, B. E. Petel and E. M. Matson, *Journal of the American Chemical Society*, 2020, **142**, 9915-9919.
81. B. E. Petel and E. M. Matson, *Chemical Communications*, 2020, **56**, 555-558.
82. E. M. M. Brittney E. Petel, *Inorganic Chemistry*, 2020, DOI: 10.1021/acs.inorgchem.0c02052.
83. A. L. Odom, C. C. Cummins and J. D. Protasiewicz, *Journal of the American Chemical Society*, 1995, **117**, 6613-6614.
84. N. E. Brese, O'Keeffe, M., *Acta Crystallographica Section B*, 1991, **47**, 192-197.
85. I. D. Brown, Wu, K. K., *Acta Crystallographica Section B*, 1976, **32**, 1957-1959.
86. W. Liu and H. H. Thorp, *Inorganic Chemistry*, 1993, **32**, 4102-4105.
87. R. H. Holm, *Chemical Reviews*, 1987, **87**, 1401-1449.
88. S. B. Yu and R. H. Holm, *Inorganic Chemistry*, 1989, **28**, 4385-4391.
89. R. R. Conry and J. M. Mayer, *Inorganic Chemistry*, 1990, **29**, 4862-4867.
90. J. Paudel, A. Pokhrel, M. L. Kirk and F. Li, *Inorganic Chemistry*, 2019, **58**, 2054-2068.
91. M. Castiñeira Reis, M. Marín-Luna, C. Silva López and O. N. Faza, *Inorganic Chemistry*, 2017, **56**, 10570-10575.
92. T. Saito, T. Sunaga, N. Sakai, Y. Nakamura, S. Yamamoto, D. Iriuchijima and K. Yoza, *Inorganic Chemistry*, 2005, **44**, 4427-4432.

93. K. Oya, H. Seino, M. Akiizumi and Y. Mizobe, *Organometallics*, 2011, **30**, 2939-2946.
94. J. S. Kanady, J. L. Mendoza-Cortes, E. Y. Tsui, R. J. Nielsen, W. A. Goddard and T. Agapie, *Journal of the American Chemical Society*, 2013, **135**, 1073-1082.
95. R. F. Hudson, Academic: New York 1965, vol. 6, pp. 68-70.
96. H. K. Wang, *Acta Chemica Scandinavica*, 1965, **19**, 879-882.
97. J. Gangopadhyay, S. Sengupta, S. Bhattacharyya, I. Chakraborty and A. Chakravorty, *Inorganic Chemistry*, 2002, **41**, 2616-2622.
98. P. Basu, B. W. Kail and C. G. Young, *Inorganic Chemistry*, 2010, **49**, 4895-4900.
99. M. N. Golovin, M. M. Rahman, J. E. Belmonte and W. P. Giering, *Organometallics*, 1985, **4**, 1981-1991.
100. C. A. Tolman, *Chemical Reviews*, 1977, **77**, 313-348.
101. M. S. Reynolds, J. M. Berg and R. H. Holm, *Inorganic Chemistry*, 1984, **23**, 3057-3062.
102. L. E. V. Anjula M. Kosswattaarachchi, Olaf Nachtigall, Joshua P. Hazelnis, William W. Brennessel, Ellen M. Matson, and Timothy R. Cook *J. Electrochem. Soc.*, 2019, **166**, A464-A472.
103. Y. Chen, Z. Wang, S. Chen, H. Ren, L. Wang, G. Zhang, Y. Lu, J. Jiang, C. Zou and Y. Luo, *Nature Communications*, 2018, **9**, 818.
104. B. Li, L. Xie, Z. Wang, S. Chen, H. Ren, Y. Chen, C. Wang, G. Zhang, J. Jiang and C. Zou, *Angewandte Chemie International Edition*, 2019, **58**, 13711-13716.
105. J. Tucher, L. C. Nye, I. Ivanovic-Burmazovic, A. Notarnicola and C. Streb, *Chemistry – A European Journal*, 2012, **18**, 10949-10953.
106. Q. Chen, D. P. Goshorn, C. P. Scholes, X. L. Tan and J. Zubieta, *Journal of the American Chemical Society*, 1992, **114**, 4667-4681.
107. V. W. Day, W. G. Klemperer and D. J. Maltbie, *Journal of the American Chemical Society*, 1987, **109**, 2991-3002.
108. G. Arana, N. Etxebarria, L. A. Fernandez and J. M. Madariaga, *Journal of Solution Chemistry*, 1995, **24**, 611-622.
109. N. Etxebarria, L. A. Fernández and J. M. Madariaga, *Journal of the Chemical Society, Dalton Transactions*, 1994, 3055-3059.
110. J. P. Launay, *Journal of Inorganic and Nuclear Chemistry*, 1976, **38**, 807-816.
111. L. P. Kazansky and J. P. Launay, *Chemical Physics Letters*, 1977, **51**, 242-245.
112. Y. Jeannin, J. P. Launay and M. A. S. Sedjadi, *Inorganic Chemistry*, 1980, **19**, 2933-2935.
113. H. Ichida, K. Nagai, Y. Sasaki and M. T. Pope, *Journal of the American Chemical Society*, 1989, **111**, 586-591.
114. M. M. Montemore, M. A. van Spronsen, R. J. Madix and C. M. Friend, *Chemical Reviews*, 2018, **118**, 2816-2862.
115. M. W. Roberts, *Chemical Society Reviews*, 1989, **18**, 451-475.
116. F. Yang, J. Graciani, J. Evans, P. Liu, J. Hrbek, J. F. Sanz and J. A. Rodriguez, *Journal of the American Chemical Society*, 2011, **133**, 3444-3451.
117. M. Shelef, K. Otto and H. Gandhi, *Journal of Catalysis*, 1968, **12**, 361-375.
118. L. Kundakovic and M. Flytzani-Stephanopoulos, *Journal of Catalysis*, 1998, **179**, 203-221.
119. Y. Moro-Oka, Y. Morikawa and A. Ozaki, *Journal of Catalysis*, 1967, **7**, 23-32.
120. S. Malkhandi, P. Trinh, A. K. Manohar, K. C. Jayachandrababu, A. Kindler, G. K. Surya Prakash and S. R. Narayanan, *Journal of The Electrochemical Society*, 2013, **160**, F943-F952.
121. Y. Zhu, X. Liu, S. Jin, H. Chen, W. Lee, M. Liu and Y. Chen, *Journal of Materials Chemistry A*, 2019, **7**, 5875-5897.
122. H. Osgood, S. V. Devaguptapu, H. Xu, J. Cho and G. Wu, *Nano Today*, 2016, **11**, 601-625.
123. S. Yan, C. DiMaggio, S. Mohan, M. Kim, S. O. Salley and K. Y. S. Ng, *Topics in Catalysis*, 2010, **53**, 721-736.
124. P. J. Denny and M. V. Twigg, in *Studies in Surface Science and Catalysis*, eds. B. Delmon and G. F. Froment, Elsevier, 1980, vol. 6, pp. 577-599.
125. Y. X. Wenliang Sun, Huizhang Liu, Jilie Kong, Songlin Jin, Gaoyang Xie, Jiaqi Deng, *Indian Journal of Chemistry Section A: Inorganic, Physical, Theoretical and Analytical*, 1997, **36**, 1023-1030.
126. W. Sun, F. Yang, H. Liu, J. Kong, S. Jin, G. Xie and J. Deng, *Journal of Electroanalytical Chemistry*, 1998, **451**, 49-57.
127. W. Sun, S. Zhang, X. Lin, L. Jin, S. Jin, J. Deng and J. Kong, *Journal of Electroanalytical Chemistry*, 1999, **469**, 63-71.
128. S. Dong, X. Xi and M. Tian, *Journal of Electroanalytical Chemistry*, 1995, **385**, 227-233.
129. C. L. Ford, Y. J. Park, E. M. Matson, Z. Gordon and A. R. Fout, *Science*, 2016, **354**, 741.
130. G. Cioncoloni, I. Roger, P. S. Wheatley, C. Wilson, R. E. Morris, S. Sproules and M. D. Symes, *ACS Catalysis*, 2018, **8**, 5070-5084.
131. C. M. Moore and N. K. Szymczak, *Chemical Science*, 2015, **6**, 3373-3377.
132. M. Kumar, N. A. Dixon, A. C. Merkle, M. Zeller, N. Lehnert and E. T. Papish, *Inorganic Chemistry*, 2012, **51**, 7004-7006.
133. R. H. Holm and J. P. Donahue, *Polyhedron*, 1993, **12**, 571-589.
134. D. D. Wagman, *The Nbs Tables of Chemical Thermodynamic Properties: Selected Values for Inorganic and C_1 and C_2 Organic Substances in Si Units.*, American Chemical Society and the American Institute of Physics for the National Bureau of Standards, Washington, DC, 1982.
135. M. L. Maiola, B. E. Petel, W. W. Brennessel and E. M. Matson, *Dalton Transactions*, 2020, DOI: 10.1039/D0DT01077D.
136. F. Li, L. E. VanGelder, W. W. Brennessel and E. M. Matson, *Inorganic Chemistry*, 2016, **55**, 7332-7334.
137. R. L. Meyer, Brennessel, W. W., Matson, E.M., *Polyhedron* 2018, **156**, 303-311.
138. L. E. VanGelder, W. W. Brennessel and E. M. Matson, *Dalton Transactions*, 2018, **47**, 3698-3704.
139. L. E. VanGelder, P. L. Forrestel, W. W. Brennessel and E. M. Matson, *Chemical Communications*, 2018, **54**, 6839-6842.

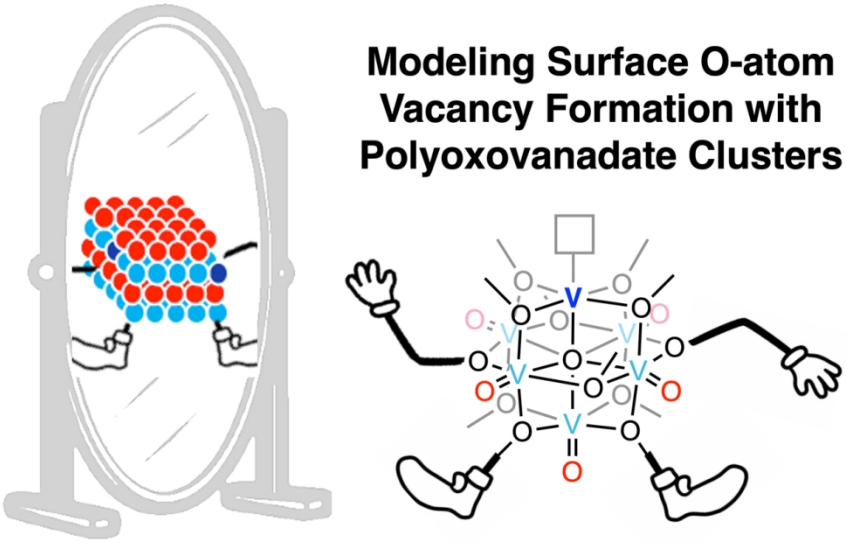

126x76mm (300 x 300 DPI)